Fire Growth in a High-rack Storage

Markus E.[1,]*, Snegirev A.[1], Kuznetsov E.[1], Tanklevskiy L.[1,2]

[1] *Peter the Great St.-Petersburg Polytechnic University, St. Petersburg, Russia*
[2] *Gefest Enterprise Group, St. Petersburg, Russia*
**Corresponding author's email: eksmarkus@gmail.com*

ABSTRACT

The mechanisms controlling the heat release growth rate and its dependency on time are studied in this work for cases of a high-rack storage facility and a single large-scale vertical PMMA slab. The latter case is considered to be a simplified set-up to get a deeper understanding of transient dynamics of the HRR growth rate and studied both theoretically and numerically. First, we modify and apply the simplified analytical model based on the classical approach, in which combustible surface is divided into the inert heating zone and the pyrolysis zone. The relationship for the flame spread is based on empirical correlations for turbulent flame length and HRR. In this work we set the turbulent flame height to be equal to the inert heating zone height and, thus, an accelerating flame spread can be predicted. Assuming that a pyrolysis front is flat and normal to the direction of propagation, the HRR growth rate for this scenario can be described using the t^3 dependence, which over-predicts the published measured values. Overall, a reasonable agreement is achieved.

Secondly, we address the same scenario with CFD simulations using FDS with finite-rate pyrolysis model. The transient HRR rate is predicted and favourably agrees the published measured data. This and and the predicted distribution of the burning rate over the burning surface justify that the pyrolysis front is in fact curviliniar.

Finally, the simplified approach is applied to predict the fire growth in the rack storage configuration. We show that a dramatically fast HRR growth rate can be observed for a large-scale scenario. A t-cube dependency of HRR growth rate is in a better agreement with FDS results than a conventional t-squared fire curve for the fast and ultrafast growth rate recommended by NFPA 204, etc. The predicted fire dynamics is analysed and the influence of the ignitor position is found to be substantial only for the initial stages of fire growth.

KEYWORDS: Flame spread, ignition, heat release rate, pyrolysis, CFD, rack storage fire, t-squared fire.

INTRODUCTION

High-rack storage fires are extremely destructive due to the very rapid growth and enormous heat release rate. An exceptionally high fire growth rate is determined by the fuel load geometry with densely packed combustible items; intense radiative exchange between the items causing its rapid ignition; the chimney-like effect generating the intensive in-rack flows and suction of fresh air into the burning region.

A designed-fire approach and the t-squared curve for the HRR rate routinely used by engineers (NFPA 72, 92B, 204, etc.) fail to reproduce the actual HRR growth rate occurring in the rack storages. Indeed, the t-squared dependence replicates the ideal scenario of symmetric expansion of the burning surface at a constant spread rate (if the burning rate is also constant). When either of the assumptions fails, the t-squared dependence becomes invalid. Clearly, if the burning zone expands

Proceedings of the Ninth International Seminar on Fire and Explosion Hazards (ISFEH9), pp. 796-807
Edited by Snegirev A., Liu N.A., Tamanini F., Bradley D., Molkov V., and Chaumeix N.
Published by Saint-Petersburg Polytechnic University Press
ISBN: 978-5-7422-6498-9 DOI: 10.18720/spbpu/2/k19-70

at an accelerating rate and/or the burning rate per unit surface area increases in time, then a higher exponent becomes appropriate in the power law to approximate the actual HRR dynamics.

The examples are the large-scale tests undertaken by Yu et al. in Refs. [1, 2], where the t^3 dependence was observed. More recent large-scale tests and simulations by Ren et al. [3] and Wang et al., Ref [4] are also consistent with this observation. To replicate the transient dynamics of the heat release rates observed in the warehouse containing high-rack storage, the exponential function was used by Alvares et al. in Ref. [5]. Even stronger dependence of the convective heat release rate on time, $\alpha\exp(\beta t)(a+bt)$, was derived by Ignason in Refs. [6, 7, 8], where the effect of a vertical flue size on the high-rack storage fire was examined.

The objective of this work is to get a deeper insight into the mechanisms controlling the HRR growth rate in the rack storage facilities. We focus on the initial stage of the fire development before the fire suppression systems are activated.

Fire growth rate in a rack storage is governed by the flame spread over the combustible surfaces. In its turn, the acceleration of the HRR growth is mainly determined by the upward flame spread over the vertical combustible surfaces. This scenario, therefore, needs to be considered in detail, both analytically and numerically. Indeed, the dynamics of the HRR growth occurring in this simplified scenario will also explain the transient fire growth rate in a realistic rack storage. Also, accelerating burning of the vertical combustible surface is an important benchmark to validate the CFD code.

In the first part of this work, we show that the t^3 dependence represents the growth rate in an upward turbulent flame spread over a vertical combustible surface, provided the pyrolysis front is flat and normal to the direction of propagation. This is done by utilising a modified version of the classical flame spread model, which is based on the simplified (thermal) pyrolysis model.

Based on the extensive CFD study, we then show that the fire growth rate in the rack storage is so fast that its approximation may require even higher order transient dependence.

UPWARD FLAME SPREAD OVER THE VERTICAL COMBUSTIBLE SURFACE

Approximate analytical model

Objective of the approximate analytical model is to provide simple relations for the transient flame spread velocity and the heat release rate when the flame propagates upwards over a vertical combustible surface. Following the classical approach [9, 10 etc.], the combustible surface is divided into two parts: the inert heating zone (where the surface temperature rises from the initial value to the ignition temperature), and the pyrolysis zone (where the surface temperature and the volatiles mass flux are assumed to be constant). The extent of the inert heating zone is set equal to the flame height, L_f, while the location of the pyrolysis front, x_p, is defined as the height at which the heating time just exceeds the time to ignition (estimated according to the thermal theory for thermally thick or thermally thin layer). Flame spread rate is then evaluated as the rate at which the pyrolysis front propagates upwards:

$$V_p = \frac{dx_p}{dt} = \frac{L_f}{\tau_{ign}}. \tag{1}$$

The turbulent flame height is evaluated using the empirical correlation proposed in Ref. [11]:

$$\frac{L_f}{W} = CQ^{*2/3}, \tag{2}$$

where W is the width of the combustible surface, C is the empirical constant, and Q^* is the non-dimensional heat release rate,

$$Q^* = \frac{\dot{Q}}{\rho_0 c_P T_0 \sqrt{g} W^{5/2}}. \tag{3}$$

In Eq. (3), ρ_0, c_P, T_0 are the density, heat capacity, and temperature of ambient air, and g is the gravity acceleration. Total heat release rate, $\dot{Q}$, is evaluated assuming the flat shape of the pyrolysis front and uniform distribution of the burning rate, m'', over the pyrolysis zone:

$$\dot{Q} = x_p W m'' f_c \Delta h_c, \tag{4}$$

where Δh_c is the heat of combustion of volatiles, and f_c is the combustion efficiency.

Substituting Eqs. (3) and (4) to Eq. (2) yields the relation for the flame length:

$$L_f = C\left(\frac{x_p m'' f_c \Delta h_c}{\rho_0 c_P T_0 \sqrt{g}}\right)^{2/3} = x_*^{1/3} x_p^{2/3}, \tag{5}$$

where

$$x_* = C^3\left(\frac{m'' f_c \Delta h_c}{\rho_0 c_P T_0 \sqrt{g}}\right)^2. \tag{6}$$

According to Eq. (5), the flame height does not depend on the surface width, W. Using Eqs. (5) and (1), we arrive at the differential equation for the coordinate of the pyrolysis front:

$$\frac{dx_p}{dt} = \frac{x_*^{1/3} x_p^{2/3}}{\tau_{ign}}. \tag{7}$$

It is worthy of note, that in Refs. [9, 10], among others, Eq. (2) is written as $x_f / W = CQ^{*2/3}$, where $x_f = x_p + L_f$. This is equivalent to replacing Eq. (7) by

$$\frac{dx_p}{dt} = \frac{x_*^{1/3} x_p^{2/3} - x_p}{\tau_{ign}}. \tag{8}$$

Consider Eq. (8) in more details. Solving Eq. (8) with the initial condition, $x_p(0) = 0$, yields:

$$x_p = x_*\left(1 - \exp\left(-\frac{t}{3\tau_{ign}}\right)\right)^3, \text{ and } V_p = \frac{x_*}{\tau_{ign}} \exp\left(-\frac{t}{3\tau_{ign}}\right)\left(1 - \exp\left(-\frac{t}{3\tau_{ign}}\right)\right)^2. \tag{9}$$

This solution shows that the size of the pyrolysis zone asymptotically approaches a constant value of x_*, while the flame spread velocity reaches its maximum at $t = (3\ln 3)\tau_{ign}$ and decreases afterwards. Clearly, such a behavior contradicts the experimental observations, which firmly indicate accelerating flame propagation [12]. This artefact is attributed to the continuously reduced size of the heating zone due to x_f increasing slower than x_p. It will be shown below that this inconsistency is avoided by using Eqs. (2) and (7).

For the velocity of steady flame spread over a sufficiently thick material layer (no burnout), the experimental correlation was suggested (for example, see [9]):

$$V_p = A x_p^n, \tag{10}$$

which implies that Eq. (1) yields finite accelerating solution, $x_p(t)$, only if $n < 1$. This is consistent with Eqs. (2) and (7), which imply $n = 2/3$. Using Eq. (10), it can be shown that $x_p = \left((1-n)At\right)^{1/(1-n)}$, $V_p = A\left((1-n)At\right)^{n/(1-n)} \sim t^{n/(1-n)}$, and

$$x_p = (1-n)V_p t\,. \tag{11}$$

Using Eqs. (7) and (10), the following relations are obtained for $n = 2/3$:

$$V_p = \frac{x_*}{\tau_{ign}}\left(\frac{t}{3\tau_{ign}}\right)^2, \tag{12}$$

$$x_p = x_*\left(\frac{t}{3\tau_{ign}}\right)^3. \tag{13}$$

Time to ignition, τ_{ign}, can be estimated using the assumption that the ignition occurs once the surface temperature attains the value of T_{ign} being exposed to a constant net heat flux, q''_{net}:

$$\tau_{ign} = \min\left(\frac{\pi}{4}\frac{kc\rho\left(T_{ign}-T_0\right)^2}{q''^2_{net}}, \frac{\delta c\rho\left(T_{ign}-T_0\right)}{q''_{net}} - \frac{1}{\pi}\frac{\delta^2}{a}\right), \tag{14}$$

where k, c, ρ are the thermal conductivity, heat capacity, and density of the material, and δ is the layer thickness. Two arguments in Eq. (14) correspond to the thermally thick and the thermally thin limits, respectively (a more accurate analytical solution is proposed in Ref. [13]).

The net heat flux allows for the incident (radiative and convective) heat flux, q''_{inc}, and the re-radiation:

$$q''_{net} = q''_{inc} - \varepsilon\sigma T_{ign}^4, \tag{15}$$

where ε is the surface emissivity.

The relations given by Eqs. (12), (13), and (14) constitute the simplified analytical model of the upward spread of a turbulent flame over a vertical combustible surface. According to Eq. (4), we obtain $\dot{Q} \sim t^3$ for the transient heat release rate. According to Eq. (13), time required for the pyrolysis zone to reach the top of the surface is $t_H = 3\tau_{ign}\left(H/x_*\right)^{1/3}$, where H is the height of the combustible surface.

To validate the model, we consider the large-scale experiment [12], in which upward flame spread over the 5 m high vertical PMMA slab (0.58 m wide, 2.5 cm thick) was studied. The lower part of the slab was exposed to the heat flux produced by the radiative panel (igniter). In the experiments [12], transient dynamics of total heat release rate, spatial distributions of surface heat fluxes, height of the pyrolysis region were recorded. Table 1 summarizes the thermal properties of the combustible material and ambient air used in the simulations to replicate the experimental conditions. Data in

Table 1 imply that the heat release rate per unit area of a burning surface is equal to $Q'' = m'' f_c \Delta h_c$ = 419 kW/m^2.

Table 1. Material properties

Material	Property	Value
PMMA	Conductivity, W/(m·K)	0.21
	Specific heat, J/(kg·K)	1500
	Density, kg/m^3	1190
	Critical mass flux, kg/(m^2·s)	0.02
	Ignition temperature, K	640
	Heat of combustion, kJ/kg	25600
	Heat of gasification, kJ/kg	700
	Combustion efficiency, –	0.82
	Emissivity, –	0.85
Ambient air	Specific heat, J/(kg·K)	1000
	Density, kg/m^3	1.1
	Temperature, K	300

To allow for the heat of gasification, Δh_g, the specific heat in Eq. (14) is multiplied by $1 + \Delta h_g \left/ \left(c\left(T_{ign} - T_0\right)\right)\right.$. Based on the literature data [9, 11] for the flame heat flux with no external heating, the incident heat flux is set q''_{inc} = 30 kW/m^2. With the model constant C = 2, Eqs. (6) and (14) yield x_* = 1.32 m, τ_{ign} = 266 s (thermally-thick limit), and Eq. (13) becomes $x_p = \alpha t^3$, where $\alpha = x_* \left/ \left(3\tau_{ign}\right)^3\right.$ = 2.59·10^{-9} m/s^3. This dependency is shown in Fig. 2, a, by the dashed line; it can be seen that the analytical model with the selected value of the model constant replicates the transient propagation of the pyrolysis front in good agreement with the experiment.

For a flat shape of the pyrolysis front (normal to the direction of spread), Eq. (4) yields the dependence, $\dot{Q} = W m'' f_c \Delta h_c \alpha t^3$, which is depicted by the dashed line in Fig. 2, b. The heat release rate predicted by the approximate analytical model exceeds that observed in the experiment [12] (the latter can be approximated by $\dot{Q}_{exp} = 2.233 \cdot 10^{-12} t^{4.7}$, kW). Such a discrepancy can be attributed to the curvilinear shape of the pyrolysis front (pyrolysis front at the periphery of the surface propagates slower than that at the central line), and, possibly, to both spatial and temporal variation of the burning rate per unit surface area.

Assuming the burning rate to be constant, the ratio of the actual pyrolysis area to that in case of the flat pyrolysis front can be estimated as $\dot{Q}_{exp} \left/ \dot{Q} = 3.62 \cdot 10^{-6} t^{1.7}\right.$. Thus, at the time instant of t_H = 1245 s (when the pyrolysis front at the central line reaches the top of the combustible surface), only 66% of the surface area is engulfed in flame in the experiment. This conclusion was also supported by the FDS simulations [14] with the finite-rate pyrolysis model. These simulations predicted curvilinear pyrolysis front, and, depending on the shape of the front, three different regimes of the flame spread were identified (see Ref. [14] for more details).

CFD MODELING

We also use the FDS software [15] to perform the simulations, in which the gaseous flame is coupled with the ignition and burning of the solid material. We apply the finite-rate single-step pyrolysis reaction, the kinetic parameters for which as well as other model settings are listed in Ref. [14]. Computational grid consists of 368640 cubic cells (2.5^3 cm^3) covering the domain (see Fig. 1, a) with the dimensions 1.2 x 0.6 x 8 m (length x width x height). The thermal properties are the same as in the previous section (see Table 1).

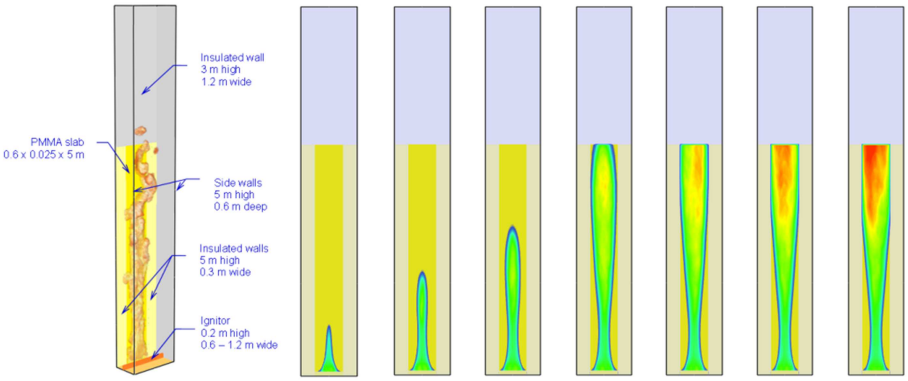

Fig. 1. Predicting upward flame spread over the vertical PMMA slab by FDS. (a) Computational domain and boundary conditions. (b) Instantaneous surface distributions of the burning rate at time instants 600, 900, 1047, 1197, 1224, 1254, and 1284 s (ignitor width 1.2 m, temperature 825 °C). Finite-rate pyrolysis model.

This computational mesh is expected to resolve the controlling length scales. In case of upward flame spread these scales are the flame height (which determines the heated area of the slab prior to ignition), and the flame thickness normal to the wall (which determines the heat flux from flame). In our previous work [14], several fine meshes (cubic cells with the dimensions of 2, 3, 5, 10, and 15 mm) were used to perform grid sensitivity analysis for the vertical porous burner (0.38 m wide, 0.792 m high) and to assess mesh resolution in the vicinity of the burner surface. As shown in Ref. [14], total (convective and radiative) heat flux from the flame can still be predicted with a reasonable accuracy if the cell size is of order of 1^3 cm^3.

In this work, three computational meshes with cubic cells of 2.5^3 cm^3 (referred as basic), 1.6^3 cm^3, and 1.25^3 cm^3 were used to conduct a grid sensitivity analysis. The total heat release rate is not affected by the grid refinement, although the computational cost increases dramatically. It takes 340 hours of the wall clock time to compute 600 s of simulation time using 24 CPU cores with the finest mesh (2 CPU Intel Xeon E5-2697 v3), which is at least four times higher than with the basic mesh. This cell size is sufficient to predict turbulent flame dynamics and flame height since the characteristic length scale, $D^* = \left(\dot{Q}/\rho_0 c_{P,0} T_0 \sqrt{g}\right)^{2/5}$, is spanned by more than 10 cells, which obeys the recommendations provided in Ref. [15].

The solid phase resolution was not specifically studied in this work as the default FDS procedure for treatment of solid phase gridding issues is considered to be reliable. The size of the first cell is automatically chosen to resolve the thickness of the heated layer in the solid material, and the mesh is stretched in the outward direction from the surface to the middle of the slab. Only a 1D heat conduction mode is used in this study. To ensure adequate coupling between gas and solid phases, the wall temperature is updated at every time step.

To initiate flame propagation, bottom part of the slab is exposed to external heat flux produced by the ignitor (hot brick) located as shown in Fig. 1, a. The hot surface of the ignitor is faced towards the slab and located at a distance of 0.2 m away from the slab surface. Two scenarios were considered in the simulations, with the ignitor width and temperature set to 0.6 m, 900 °C, and 1.2 m, 825 °C. As shown in Fig. 2, the finite-rate pyrolysis model replicates the experimental dynamics of flame spread and HRR growth to a good accuracy. More information on the influence of the ignitor parameters on the fire dynamics is provided in Ref. [14].

Furthermore, dissimilar to the approximate analytical model, the CFD model predicts transient dynamics of the heat release rate, which is in favorable agreement with the measurement data reported in Ref. [12]. This is consistent with the observation that predicted shape of the pyrolysis zone is curvilinear, and the distribution of the burning rate over the burning surface is non-uniform as shown in Fig. 1, b (note also that the peak value increases in time as the flame size is growing).

It can therefore be concluded that the growth rate of the fire driven by the upward flame spread is higher than that corresponding to the t-squared fire. The best fit to the experimental data [12] yields $n = 4.7$, while the approximate analytical model predicts $n = 3$.

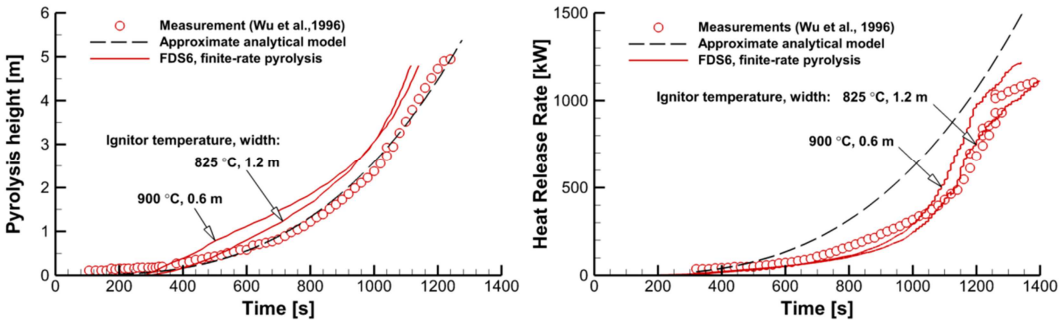

Fig. 2. Upward flame spread over the vertical PMMA slab: elevation of the pyrolysis front at the axis (a) and the heat release rate (b) as a function of time (FDS data is smoothed).

HIGH RACK STORAGE FIRE SIMULATIONS

Model setup

The above analysis shows good ability of the FDS software in predicting upward spread of the turbulent flame over the vertical combustible surface. It is expected that the simplified (thermal) pyrolysis model (consistent with the assumptions made in the approximate analytical model described in the previous section) should also be capable of predicting the experimental dynamics of flame spread, provided the model parameters are properly calibrated. Indeed, in Ref. [16] we demonstrate it for the fire growth in the rack with 2x4x3 combustible boxes and show that the predicted heat release rate is in reasonable agreement with that measured in the full-scale tests [3, 4]. The guidance on how to select to select the model parameters to fit the measurement data on the transient heat release rate is also provided in Ref. [16].

Here we apply this approach to predict the fire growth rate in the high-rack storage facility if the fire suppression system is not activated. We consider three double rows racks, 6 boxes wide array with 11-tier height each (see Fig. 3). Each box has dimensions of 0.8x1.2x1.0 m, horizontal and vertical flues are 0.1 and 0.4 m, respectively, the distance between the rows in one rack is 0.5 m, and the distance between the racks is 3.54 m. For simplicity, we do not take into account wooden pallets,

which are often used in practice. Each box is treated as a solid obstruction, and the thermal pyrolysis model is applied as the boundary condition at the box sides.

Model input parameters are retained the same as those in Ref. [16] and summarized in Table 2. These model parameters were selected in the iterative procedure which includes (i) evaluation of the literature data on material thermal properties and ignition temperature, (ii) estimation of HRRPUA and burnout time based on the HRR measurements, and (iii) calibration of the heat of gasification. With these model parameters, the measured heat release rate produced by burning of the corrugated cardboard boxes in the validation experiments [4] was reasonably replicated in FDS simulations with the simplified (thermal) pyrolysis model [16].

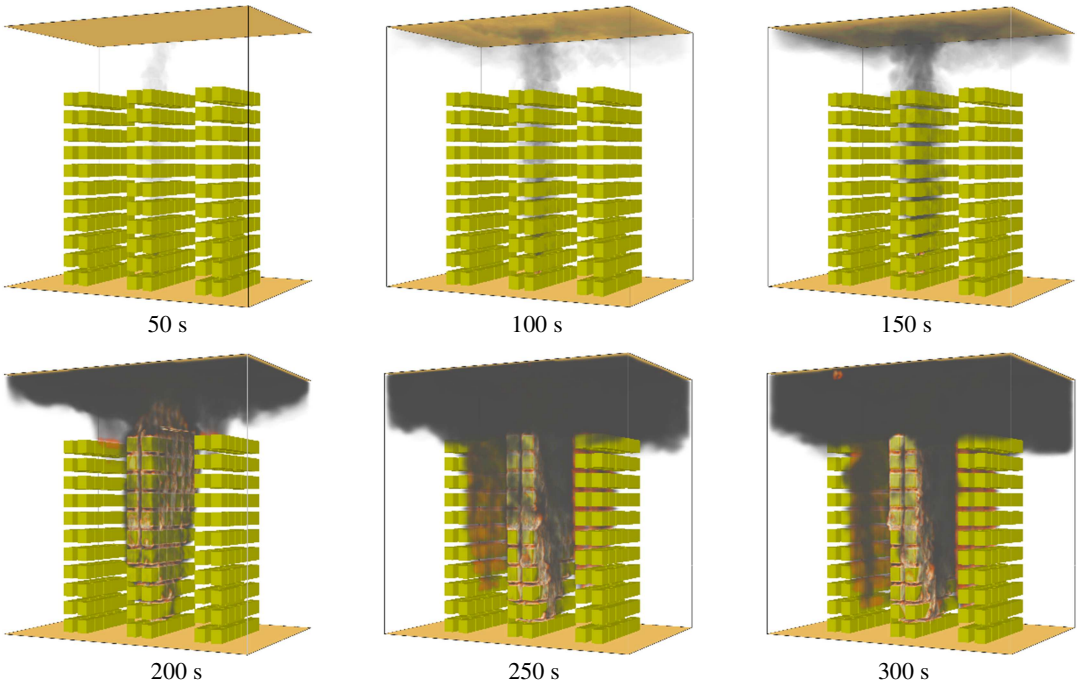

Fig. 3. FDS predictions of the fire development in the high-rack storage: instantaneous iso-surfaces of 200 kW/m^3 heat release rate and soot mass fraction at 50-300 s.

Table 2. Model parameters for the high-rack storage fire simulations

Material	Property	Value
Corrugated double wall cardboard	Conductivity, W/(m·K)	0.1
	Specific heat, J/(kg·K)	2700
	Density, kg/m^3	184
	Ignition temperature, K	633
	Heat of combustion, kJ/kg	14200
	Heat of gasification, kJ/kg	1000
	Emissivity, –	0.9
	HRRPUA, kW/m^2	200
	Burnout time, s	290
	Layer thickness, m	0.022

The fire is initiated by the ignitor, which is represented by the rectangular box with the dimensions of 0.4x0.6x0.3 m^3, located at the bottom of the central rack. The ignitor heat release rate rises from 0 to $\dot{Q}_{0,\max}$ = 1 MW according to the expression $\dot{Q}_0 = \min\left(\alpha_0 t^2, \dot{Q}_{0,\max}\right)$, where α_0 = 0.011 kW/s^2. Three ignitor positions are considered as illustrated in the inset in Fig. 4 and referred hereafter as cases 1, 2, and 3.

The computational domain is unconfined (side boundaries are open) and has the dimensions of 20x14x20 m^3. The central rack area is spanned with 5^3 cm^3 cubic cells. A coarser grid with 10^3 cm^3 cubic cells is used in the space between the racks and above the central rack (which corresponds to the main plume). The coarsest grid with 20^3 cm^3 cubic cells is used around the side racks. In spite of the rather large grid cells, the total number of cells is considerable (5145600), which is due to the large sizes of the domain. Simulation of 200 s physical time took 20 hours of CPU time with 84 cores of 2 Intel Xeon E5-2697 v3, 2.60 GHz processors.

Due to the large size of the domain compared to the length scales of horizontal and vertical flues, it is extremely expensive to conduct a comprehensive grid sensitivity analysis, which requires meshes with tens of millions of grid cells. However, our previous work, see Ref. [16], have shown that a quantitative agreement of the predicted dynamics of the heat release rate with that measured in the FM Global rack storage fire scenario ((2x4x3 boxes in the rack, horizontal flue 15 cm, vertical flue 46 cm, see Refs. [3, 4]) can still be obtained with the comparable grid resolution (2.5^3 cm^3 cubic cells in the central rack area). For the high-rack storage facilities, validation data is not available, and the predictions made in this work should be regarded as qualitative.

Simulation results

As shown in Fig. 4, the ignitor position greatly affects the overall HRR dynamics which is determined by the ventilation conditions and the distances between the combustible surfaces. The fastest fire development is observed when the ignitor is placed below and between two boxes, just below the narrow vertical flue (see case 2 in the inset in Fig. 4). In this case, a small distance between the boxes leads to intensive radiative exchange between and rapid ignition of the adjacent surfaces, while the vertical flue above the ignitor promotes fast upward flame spread over the vertical side surfaces of the boxes, jointly with the intensive air entrainment due to the chimney-like effect.

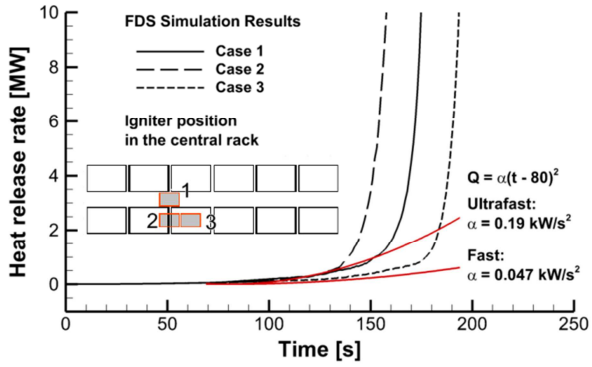

Fig. 4. Predicted heat release rate time dependences (cases 1, 2, 3 – ignitor locations).

In contrast, the longest delay of the HRR growth rate is observed if the ignitor is located centrally beneath the box, away from the vertical flues (see case 3 in Fig. 4). In this case, the upward flame spread is delayed for the time needed for the flame to engulf the bottom of the adjacent box just above the ignitor.

In case 1 the igniter is located in the centre of the rack between the rows, i.e. in the wide vertical flue (see the inset in Fig. 4). In this case, the ventilation and geometrical conditions are favourable for upward flame spread, but, on the other hand, the larger distance between the combustible surface implies less intensive radiative exchange than that in case 2, and this explains the longer times to ignition and the longer delay in the HRR runaway.

A typical predicted fire dynamics is illustrated by the instantaneous flame shapes and smoke concentrations shown in Fig. 3 for case 1. Similar to Refs. [3, 4, 16], the following stages of fire development can be identified. First, at time instant 80 s the vertical surfaces of the boxes of the first tier are ignited. Then the flame propagates upward over the vertical surfaces of the boxes facing inside the rack. At 160 s, the plume starts to widen and the flame spreads over the horizontal surfaces of the 2nd to 6th tiers. At 180 s, the flame spreads over the vertical surfaces of the boxes in 5th and 6th tiers. At about 190 s, all the surfaces of the 7th to 10th tiers are engulfed in fire. High irradiation leads to ignition of vertical surfaces of the 11th tier of the side racks, the flame then starts to spread downwards. At 250 s, all the boxes of the central rack at the level of 5th to 11th tiers burn. At 300 s flame spreads over the horizontal surfaces at the side racks.

Thus, the time periods of primarily vertical flame spread are followed by the time periods when the flame also propagates horizontally over the box surfaces. In the catastrophic case when the fire suppression system is not activated, radiative ignition of the upper tiers of the side racks occurs eventually. This is followed by the downward flame propagation, which is slower than the upward flame spread in the central rack.

As the fire develops, the effect of the ignitor location ceases, and the above listed stages of the fire growth remain to be almost the same, as well as the rate at which the HRR grows. Thus, for the three ignitor locations considered in this work, the difference is mainly in the initial delay of the HRR runaway.

It is worthy of note, that the predicted HRR rises extremely rapidly. Clearly, the t-squared fire curves shown by the red solid lines for the fast and ultrafast growth rate (as classified by NFPA 204) fail to replicate the HRR growth rates characteristic of the rack-storage fires. The predicted HRR growth rates can still be approximated by the power-law, $\dot{Q} \sim (t - t_0)^n$, where the value of n is in the range from 3 to 6 depending on the selected value of the incubation period, t_0. In particular, if the incubation period of t_0 = 130 s is assumed, then the good fit is provided by n = 3.

CONCLUSIONS

Fire growth for two scenarios of practical importance is considered in this work and particular attention is given to high-rack storage fires and the mechanisms controlling the heat release growth rate and its dependency on time, which is found to be stronger than the conventional t-squared fire curves recommended by NFPA 204, etc. Provided that the fire growth during initial stages, i.e. before the suppression system is activated, is governed mainly by the upward flame spread propagation we first examine a simplified scenario addressing the upward flame spread over a continuous 5 m high PMMA slab both numerically and theoretically. Indeed, the dynamics of the HRR growth occurring in this simplified scenario also explains the transient fire growth rate in a realistic rack storage.

First, we modify and apply the simplified analytical model, in which combustible surface is divided into the inert heating zone and the pyrolysis zone. The relationship for the flame spread is based on empirical correlations for turbulent flame length and HRR. In this work we set the turbulent flame height to be equal to the inert heating zone height and, thus, an accelerating flame spread can be predicted. Assuming that a pyrolysis front is flat and normal to the direction of propagation, the

HRR growth rate for this scenario can be described using the t^3 dependence, which exceeds the published measured values [12].

Secondly, we address the same scenario with CFD simulations using FDS with finite-rate pyrolysis model. The transient HRR rate is predicted and favourably agrees the published measured data. This and the predicted distribution of the burning rate over the burning surface, which found to be non-uniform and transient in time, justify that the pyrolysis front is in fact curviliniar, which explains why the analytical model over-predicts the HRR growth rate for the same scenario. The growth rate of the fire driven by the upward flame spread in this case is higher than that corresponding to the t-squared fire. The best fit to the experimental data [12] yields $n = 4.7$, while the approximate analytical model predicts $n = 3$. Regimes and mechanisms of flame spread are also examined and found to be depended on the igniter properties and size, the analysis of which can be found elsewhere [14].

Finally, the simplified approach is applied here to predict the fire growth in the rack storage configuration. The predicted fire dynamics is analysed and the influence of the ignitor position is found to be substantial only for the initial stages of fire growth. The time periods of primarily vertical flame spread are followed by the time periods when the flame also propagates horizontally over the box surfaces. In the catastrophic case when the fire suppression system is not activated, radiative ignition of the upper tiers of the side racks occurs eventually. This is followed by the downward flame propagation, which is slower than the upward flame spread in the central rack. We show that a dramatically fast HRR growth rate can be observed for this large-scale scenario, which, however, still can be described using the power-law function $\dot{Q} \sim (t - t_0)^n$. In particular, if the incubation period of 130 s is assumed, a t-cube curve is in a better agreement with FDS results than a conventional t-squared fire curve for the fast and ultrafast growth rate (as classified by NFPA 204).

ACKNOWLEDGEMENT

This work is supported by RSF (project 16-49-02017). Simulations were performed at the supercomputer center “Polytechnic” (SPbPU).

REFERENCES

[1] H.-Z. Yu. Transient Plume Influence in Measurement of Convective Heat Release Rates of Fast-Growing Fires Using a Large-Scale Fire Products Collector, J. Heat Transfer 112 (1990) 186-191.

[2] H.-Z. Yu, P. Stavrianidis. The Transient Ceiling Flows of Growing Rack Storage Fires. In: Cox G., Langford B. (Ed.), Fire Safety Science – Proceedings of the Third International Symposium, pp. 281-290, 1991.

[3] N. Ren, J. de Vries, X. Zhou, M. Chaos, K. V. Meredith, Y. Wang, Y. Large-Scale Fire Suppression Modeling of Corrugated Cardboard Boxes on Wood Pallets in Rack-Storage Configurations, Fire Safety J. 91 (2017) 695–704.

[4] Y. Wang, K. V. Meredith, X. Zhou, P. Chatterjee, Y. Xin, M. Chaos, N. Ren and S. B. Dorofeev. Numerical Simulation of Sprinkler Suppression of Rack Storage Fires. In: Nilsson D., van Hees P., Jansson R. (Ed.), Fire Safety Science – Proceedings of the Eleventh International Symposium, IAFSS, pp. 1170–1193, 2014.

[5] N. J. Alvares, H. K. Hasegawa, K. Hout, A. C. Fernandez-Pello, J. White, Analysis of a Run-Away High Rack Storage Fire. In: Kashiwagi T. (Ed.), Fire Safety Science – Proceedings of the Fourth International Symposium, IAFSS, pp. 1267-1278, 1994.

[6] H. Ingason, Heat Release Rate of Rack Storage Fires, Proceedings of 9th Interflam 2001 Fire Science & Engineering Conference, p. 731-740, 2001.

[7] H. Ingason, In-Rack Fire Plumes. In: Evans D. D. (Ed.), Fire Safety Science – Proceedings of the Fifth International Symposium, IAFSS, pp. 333–344, 2003.

[8] H. Ingason. Effects of Flue Spaces on the Initial In-Rack Plume Flow. In: Evans D. D. (Ed.), Fire Safety Science – Proceedings of the Seventh International Symposium, IAFSS, pp. 235-246, 2003.

[9] J.G. Quintiere. Surface Flame Spread. In: SFPE Handbook of Fire Protection Engineering, 2nd Ed. NFPA, 2002. p. 2-246 – 2-257.

[10] Y. Hasemi, Surface Flame Spread, in: M.J. Hurley (Ed.), SFPE Handbook of Fire Protection Engineering, Springer, New York, NY, 2016, pp. 705-723.

[11] J. G. Quintiere, T. G. Cleary, Heat Flux from Flames to Vertical Surfaces, Fire Technol. 30 (1994) 209–231.

[12] P.K. Wu, L. Orloff, A. Tewarson. Assessment of Material Flammability with the FSG Propagation Model and Laboratory Test Methods, 13th Joint Panel Meeting of the UJNR Panel on Fire Research and Safety, NIST Report NISTIR 6030, Gaithersburg, MD, USA, 1996.

[13] A. Snegirev, E. Kuznetsov, E. Markus. Coupled Analytical Approach to Predict Piloted Flaming Ignition of Non-Charring Polymers. Fire Safety Journal 93 (2017) 74-83.

[14] E. S. Markus, E. A. Kuznetsov, A. Yu. Snegirev. Buoyant Turbulent Diffusion Flame near a Vertical Surface Combustion, Explosion, and Shock Waves. 54 (2018) 284-293.

[15] K. McGrattan, S. Hostikka, R. McDermott, J. Floyd, M. Vanella. Fire Dynamics Simulator, Technical User's Guide. NIST Spec. Publ. 1019, 6th ed., 2018.

[16] E. Markus, A. Snegirev, E. Kuznetsov, L. Tanklevskiy. Application of a Simplified Pyrolysis Model to Predict fire Development in Rack Storage Facilities. J. Physics: Conf. Series 1107 042012– Proceedings of the Third European Symposium on Fire Safety, 2018.